Published in final edited form as:

Cancer Lett. 2024 December 01; 606: 217302. doi:10.1016/j.canlet.2024.217302.

Histone deacetylase upregulation of neuropilin-1 in osteosarcoma is essential for pulmonary metastasis

Niveditha Nerlakanti[a,b], **Jeremy J. McGuire**[a,b,2], **Ryan T. Bishop**[b], **Mostafa M. Nasr**[a,b], **Tao Li**[b], **Damon R. Reed**[c,1], **Conor C. Lynch**[b,*]

[a]Cancer Biology Ph.D. Program, University of South Florida, Tampa, FL, 33612, USA

[b]Department of Tumor Microenvironment & Metastasis, H. Lee Moffitt Cancer Center and Research Institute, Tampa, FL, 33612, USA

[c]Sarcoma Department, H. Lee Moffitt Cancer Center & Research Institute, Tampa, FL, 33612, USA

Abstract

The lungs represent the most common site of metastasis for osteosarcoma (OS). Despite our advances in developing targeted therapies for treating solid malignancies, broad acting chemotherapies remain the first line treatment for OS. In assaying the efficacy of approved therapeutics for non-OS malignancies, we previously identified the histone deacetylase 1 and 2 (HDAC1 and 2) inhibitor, romidepsin, as effective for the treatment of established lung metastatic OS. Yet, romidepsin has noted toxicities in humans and so here we aimed to define the primary mechanisms through which HDAC1/2 mediate OS progression to identify more selective druggable targets/pathways. Microarray and proteomics analyses of romidepsin treated OS cells revealed a significant suppression of neuropilin-1 (NRP1), a known regulator of cancer cell migration and invasion. Silencing of *NRP1* significantly reduced OS proliferation, migration,

*Corresponding author. Department of Tumor Microenvironment & Metastasis, H. Lee Moffitt Cancer Center and Research Institute, 12902 Magnolia Drive, Tampa, FL, 33612, USA. conor.lynch@moffitt.org (C.C. Lynch).
[1]Current address: MSK Kids, Memorial Sloan Kettering Cancer Center, 1275 York Ave. Street, New York, NY 10065, USA.
[2]Current address: Department of Surgery, Cancer Control, University of Rochester Medicine, 601 Elmwood Ave, Rochester, NY 14642, USA.

CRediT authorship contribution statement

Niveditha Nerlakanti: Writing – review & editing, Writing – original draft, Visualization, Validation, Software, Resources, Methodology, Investigation, Formal analysis, Data curation, Conceptualization. **Jeremy J. McGuire:** Writing – review & editing, Formal analysis. **Ryan T. Bishop:** Writing – review & editing, Formal analysis. **Mostafa M. Nasr:** Writing – review & editing, Formal analysis. **Tao Li:** Writing – review & editing, Validation. **Damon R. Reed:** Writing – review & editing, Funding acquisition, Data curation. **Conor C. Lynch:** Writing – review & editing, Writing – original draft, Visualization, Supervision, Funding acquisition, Conceptualization.

Author conflicts of interest

Dr. Damon Reed has served on the data safety monitoring committees (DSMC) for Spring Work and Eisai. All other authors have nothing to disclose.

Declaration of competing interest

The authors declare the following financial interests/personal relationships which may be considered as potential competing interests: Dr. Damon Reed has served on the data safety monitoring committees (DSMC) for Spring Work and Eisai. All other authors have nothing to disclose.

Appendix A. Supplementary data

Supplementary data to this article can be found online at https://doi.org/10.1016/j.canlet.2024.217302.

invasion and adhesion *in vitro*. More strikingly, *in vivo*, reduced NRP1 expression significantly mitigated the lung metastatic potential of OS in two independent models (K7M2 and SAOS-LM7). Mechanistically, our data point to NRP1 mediating this effect via the down regulation of migration machinery, namely SRC, FAK and ROCK1 expression/activity, that is in part, related to NRP1 interaction with integrin beta 1 (ITGB1). In summary, our data indicate that romidepsin down regulation of NRP1 significantly mitigates the ability of OS cells to seed the lung and establish metastases, and that targeting NRP1 or its effectors with selective inhibitors may be a viable means with which to prevent this deadly aspect of the disease.

Keywords

Osteosarcoma; Lung metastasis; Neuropilin-1; Histone deacetylase; SRC; ROCK; Invasion and metastasis

1. Introduction

Osteosarcoma (OS) is the most common primary bone cancer and largely affects adolescents and young adults [1]. Present standard of care for OS includes neoadjuvant therapy with a methotrexate, doxorubicin and cisplatin (MAP) combination followed by local control surgery and additional chemotherapy [2-4]. This treatment paradigm has changed little over the past four decades. Consequently, mortalities have remained largely static with five-year overall survival for primary disease at 70% but for patients with evidence of lung metastasis, the rate drops to 30% [2,5-7]. Therefore, we need new therapeutics for OS treatment that can potently block lung metastasis or treat established lung metastatic disease. One of the bottlenecks for the development of new therapies is the fact that OS is rare, with approximately 1000 new cases diagnosed each year in the US, making robust clinical trials challenging to coordinate [1,8]. Thus, strong pre-clinical data is necessary to motivate clinical trials, and there are many ongoing efforts in this area [9-13].

To address this, we previously screened 54 FDA approved drugs against five different osteosarcoma cell lines [14]. We identified panobinostat and romidepsin, FDA approved for multiple myeloma and cutaneous T-cell lymphoma respectively, to be potent inhibitors of osteosarcoma growth and metastasis *in vitro* and *in vivo* and specifically that HDAC1 and 2 are key for OS growth [15]. Panobinostat and romidepsin, while efficacious, have noted adverse effects and toxicities in patients that in turn greatly impact patient quality of life [16-18]. Therefore, we reasoned that understanding the mechanisms through which HDAC inhibitors blocked OS progression and metastasis could yield more selective druggable targets. Microarray and proteomic analyses of romidepsin treated OS cells revealed a significant downregulation of neuropilin-1 (NRP1). NRP1 acts as a co-receptor for several factors to enhance their cellular effects, such as semaphorin family members to aid axonal migration of neurons [19,20], vascular endothelial growth factor (VEGF), to facilitate angiogenesis [21,22] and hepatocyte growth factor (HGF) that mediates cell migration and invasion via the receptor tyrosine kinase, mesenchymal-epithelial transition factor (c-MET) [23-28]. NRP1 can also bind to integrins and extracellular matrix receptors to regulate cell adhesion [28,29]. Given that NRP1 is upregulated in several cancers, we investigated

whether its inhibition was the primary means through which romidepsin was exerting its efficacy [30-33]. Here, using genetic approaches, we demonstrate that NRP1 is critical for the successful metastasis and establishment of OS cells in the lungs and mechanistically, this is in part due to NRP1 control of OS cell migration machinery.

2. Results

2.1. Effect of romidepsin on genome-wide transcription and protein targets in osteosarcoma

To identify key molecular targets through which HDACs control osteosarcoma growth and metastasis, we performed genome wide expression analysis subsequent to treating SAOS2 and MG63 cell lines with romidepsin for 24h at a sub cytotoxic concentration of 200 ng/ml. Using a log2 fold cut-off, we identified significant differential gene expression in each cell line but of these only 20 upregulated genes and 16 downregulated genes were common to both (Fig. 1A-C). We also used proteomics to further understand the effect of romidepsin on protein content using the SAOS2 model. Analogous to gene expression, proteomics revealed 15 upregulated genes and 10 downregulated targets common between the microarray and proteomics datasets (Fig. S1A). Pathway enrichment analysis (EnrichR) also demonstrated altered biological processes involved in cancer metastasis such as extracellular matrix organization and regulation of cell migration in response to romidepsin (Fig. S1B). Using qRT-PCR, we subsequently validated several targets of interest and observed romidepsin dose dependent upregulation of *SH3GL2*, *SLC17A7*, *SPAG9*, *DHRS2*, *GMPR*, and downregulation of *KIT*, *MMP14*, *NRP1*, *HMGB2*, *TRIM8* (Fig. 1D and E). For translational purposes, we focused on genes whose expression were inhibited by romidepsin treatment, the rationale being that these targets would be highly expressed in OS patients and therefore could be potentially targeted with selective reagents. To that end, we interrogated the St. Jude PeCan OS patient gene expression (RNA-Seq) dataset and found *MMP14* (matrix metalloproteinase 14), *NRP1* (neuropilin-1) and *TRIM8* (tripartite motif containing protein 8) expression levels to be significantly upregulated in osteosarcoma patients (OS) compared to other pediatric cancers (Fig. 1F). Of these genes, we focused specifically on *NRP1* given that OS patients with high expression of *NRP1* have poorer overall prognosis and that functionally NRP1 is involved in multiple physiological and pathological processes [30,34-36].

2.2. Neuropilin-1 (NRP1) drives osteosarcoma growth, migration, and invasion in vitro

To define a potential role for NRP1 in osteosarcoma progression and metastasis, we initially genetically ablated its expression using an siRNA approach in the luciferase expressing metastatic SAOS-LM7 and the MG63 OS human cell lines (Figs. S2A-F). Using luminescence as a correlate for cell growth, we noted that NRP1 silencing significantly reduced the growth of both OS cell lines *in vitro* (Figs. S2G and H). We confirmed the effect of mitigating NRP1 expression on cell growth by generating control and stable NRP1 shRNA knockdowns in the metastatic OS cell lines, SAOS-LM7 and K7M2 (mouse) (Fig. 2A-F). Consistent with known roles for NRP1, we observed NRP1 knockdown OS cells also had a significantly lower ability to migrate in transwell assays and invade through matrigel coated membranes (Fig. 2G-J) [34]. Of note, reduced NRP1 levels did not mitigate

the efficacy of romidepsin, which was expected given the wide array of genes regulated by HDAC1 and 2 (Fig. S2I). However, we chose to interrogate NRP1 further given its potential regulation of OS growth and migration/invasion.

2.3. NRP1 is essential for the establishment of lung metastatic osteosarcoma in vivo

To evaluate the role of NRP1 in osteosarcoma lung metastasis *in vivo*, we used immunocompetent BALB/c mice that are syngeneic to the K7M2 OS cell line. When injected via tail vein, K7M2 yields aggressive lung metastatic OS disease and mice reach endpoint (weight loss, labored breathing, lethargy, hunched posture) in approximately 30 days (Fig. 3A) [15]. Next, we compared the ability of control or NRP1 knockdown K7M2 to metastasize to the lungs of inoculated mice (n = 7/group). Over time, we noted a decrease in body weight in the control versus NRP1 knockdown group, and at study endpoint, gross analysis of resected lungs revealed extensive macro-metastases in the controls (Avg. 62 metastases/lung) whereas no macro-metastases were detected in the NRP1 shRNA K7M2 group (0 metastases/lung) (Fig. 3B and C). Pathologist analysis of tissue sections derived from each group supported this observation with no metastases detected in any of the NRP1 shRNA K7M2 inoculated animals (Fig. 3D). For robustness, we repeated this study in immunocompromised NSG mice with SAOS-LM7 using a similar experimental design (Fig. S3A). Our findings from these studies were consistent with those derived from the K7M2 studies, with control SAOS-LM7 mice (n = 6) demonstrating on average approximately 100 number gross lung metastases at study endpoint (Day 77) while no metastases were observed in the NRP1 shRNA SAOS-LM7 group (n = 6) (Fig. S3B). However, unlike K7M2 studies, we did observe a low number of micro-metastases (0.07 % of the total lung area) in lungs sections derived from the NRP1 shRNA SAOS-LM7 group compared to controls (51 % of the total lung area; Fig. S3C).

The slower growth rates of the NRP1 shRNA cells noted *in vitro* could translate to longer times for overt metastases to form. We therefore repeated the study to determine overall survival differences between BALB/c mice tail-vein inoculated with control shRNA (n = 6) and NRP1 shRNA K7M2 (n = 7) (Fig. 4A). Our analyses showed a significant loss in body weight in the control group over the course of the study compared to those in the NRP1 shRNA group (Fig. 4B). At study endpoint, mice in the control group had a median survival time of 32.5 days which is in keeping with our previous observations for this model [15]. In contrast, none of the NRP1 shRNA inoculated group exhibited study endpoint criteria and survived until study termination at day 97 (Fig. 4C). Analysis of macro and micro metastases again revealed no evidence of lung metastases in the NRP1 shRNA K7M2 OS inoculated mice compared to the control cohort (Fig. 4D and E). These data suggest NRP1 is necessary for successful OS metastasis and establishment in the lung microenvironment.

2.4. NRP1 knockdown leads to reduced osteosarcoma primary tumor engraftment

To identify whether NRP1 was critical for establishment only in the lung microenvironment. BALB/c mice were orthotopically inoculated with control shRNA (n =6) or NRP1 shRNA (n =5) K7M2 cells (1×10^5 cells/tibia) (Fig. 5A). In previous experiments with this model, we identified that the average time for K7M2 to cause limb paralysis/cortical bone breakthrough is approximately 27 days [15]. We therefore ended the study at this time point and collected

tumor bearing tibias as well as lungs to assess spontaneous metastasis. Our data shows 100 % (6/6) engraftment in all mice that were inoculated with control shRNA K7M2 cells while only 20 % of mice (1/5) inoculated with the NRP1 shRNA K7M2 cell line showed evidence of tumor establishment and growth (Fig. 5B and C). We detected no spontaneous metastases in the lungs of the NRP1 shRNA group (0/5) in comparison to 83.3 % (5/6) of the control group (Fig. 5D and E). These data indicate that NRP1 is also critical for engraftment and potentially progression of OS in the bone microenvironment.

2.5. NRP1 controls OS migration via SRC and ROCK

Neuropilin-1 (NRP1) is a co-receptor for tyrosine receptor kinases and integrins and can enhance cell proliferation, migration, invasion and survival pathways [24,26-28]. However, its function as a target of HDAC inhibition in osteosarcoma has not been described previously. To define potential mechanisms through which NRP1 drives OS metastasis we determined, based on the literature, whether NRP1 depletion would impact the expression and/or activity of effectors such as Mothers against decapentaplegic homolog 2 (SMAD2), SMAD3, integrin B1 (ITGB1), ITGB3 and signaling molecules involved in cell migration and invasion pathways (Proto-oncogene tyrosine-protein kinase Src (SRC), Focal Adhesion Kinase (FAK), AKT serine/threonine kinase 1 (AKT1), Rho-associated coiled-coil containing protein kinase 1 (ROCK1), ROCK2, Coflin-1 (CFL1), CFL2, Rac Family Small GTPase 1 (RAC1) and Ras Homolog Family Member A (RhoA)). qRT-PCR analysis revealed decreased expression of candidate genes in the NRP1 shRNA K7M2 cells including SMAD2, SRC, FAK, ROCK1, ROCK2 (Fig. 6A). Kinase array analysis also confirmed lower levels of SRC in the shRNA NRP1 depleted K7M2 cells compared to controls (Fig. 6B). We next examined the protein levels of common downstream effectors of SRC at the basal level under serum free conditions and in response to serum addition at timed intervals. Of the candidate molecules assessed, our data demonstrated significantly reduced SRC, phospho-FAK, FAK and ROCK1 levels in the NRP1 shRNA K7M2 cells compared to controls (Fig. 6C). Interestingly, the majority of these effects were present even under serum free conditions (time 0). To determine the importance of SRC in mediating NRP1 migration, we used a pharmacological approach (dasatinib). We initially conducted an IC_{50} assay and interestingly, found that despite lower levels of SRC, dasatinib had a similar effect on the viability of control and shRNA NRP1 K7M2 (Fig. 6D). However, at a concentration below the IC_{50} for both groups (500 nM), control shRNA cell lines exhibited significantly reduced migration to a level comparable to that of the shRNA NRP1 vehicle group, while treatment of the shRNA NRP1 group with dasatinib further reduced migration compared to all other groups (Fig. 6E).

To identify potential mechanisms of NRP1 action, we focused on ITGB1 since integrins are known to play a role in cell migration and invasion via downstream activation of receptor tyrosine kinases like SRC and FAK. Further, reports show that blocking ITBG1 with neutralizing antibodies had no effect on primary tumor growth but significantly reduced the incidence of lung metastasis [37-39]. We observed that NRP1 knockdown in OS leads to reduction of ITGB1 at both mRNA and protein expression levels (Figure S4A and Fig. 6F). Interestingly, we noted that silencing ITGB1 expression reduced pSRC levels in control shRNA cells combined with a modest reduction in total SRC (Fig. 6F and Figs. S4B and C).

By comparison, NRP1 shRNA OS cells had a modest decrease in pSRC but the decrease in total SRC was more robust and combining NRP1 knockdown with ITGB1 silencing resulted in further reductions in both pSRC and SRC levels. Notably, ITGB1 silencing did not impact FAK or ROCK1 levels suggesting that NRP1 interaction with other receptors at the cell surface regulates the activity of these kinases (Fig. S4D). We also examined cell adhesion given the importance of integrins in this process. We observed that antibody neutralization of ITGB1 reduced the adherence of control OS cells to that of the NRP1 shRNA IgG treated cells while no effect with ITGB1 blockade was noted in the NRP1 shRNA group (Fig. 6G).

For clinical relevance, we re-examined the PeCan database and divided OS patients based on their expression of NRP1 (low vs. high; Fig. S4E). While SRC and FAK expression was increased in OS patients with high levels of NRP1, statistical significance was not achieved. However, ROCK1 and 2 levels were found to be significantly increased in the NRP1 high expressing groups. Taken together, these data indicate that NRP1 activation of the SRC pathway is an important driver of OS migration and likely plays a role in OS pulmonary metastasis and establishment.

3. Discussion

Osteosarcoma patients typically succumb to lung metastatic disease [40]. We previously observed that HDAC inhibition with panobinostat or romidepsin is an effective means with which to prevent and treat pulmonary metastases in pre-clinical OS models [15]. However, because of the associated toxicity of HDAC inhibition, here we focused on identifying potential drug targetable mechanisms through which HDACs facilitated osteosarcoma progression and metastasis. Using combined unbiased gene expression and proteomics approaches, we identified a number of romidepsin targets and focused primarily on NRP1 given its known roles in cancer and increased expression in osteosarcoma clinical samples [30,34-36]. Using genetic approaches, we found that NRP1 was critical for the metastasis of OS cells to the lung and that mechanistically, this may potentially be mediated via signaling through SRC activation of downstream effectors including FAK and ROCK1. While SRC inhibitors such as dasatinib have had mixed results in clinical trials for the treatment of sarcomas including lung metastatic OS, our data suggest targeting of NRP1 itself maybe more clinically effective for preventing and treating OS lung metastases [41].

Conducting clinical trials in osteosarcoma is challenging given that it is a rare cancer and requires the coordination of multiple institutes globally to enroll sufficient numbers of patients. To address this, we previously examined a panel of FDA approved drugs across a variety of OS cell lines to identify potent OS cytotoxic agents [14]. This led to our focus on the HDAC inhibitors panobinostat and romidepsin that we subsequently showed to be highly effective for the prevention and treatment of lung metastatic OS [42-44]. Unfortunately, HDAC inhibitors are not well tolerated and have associated off target toxicities that limit their use. However, we reasoned that understanding the molecular programs through which HDACs regulate cancer progression could yield more precision targets for treatment. HDACs have been reported as being involved in controlling several hallmarks of cancer components including apoptosis, cell cycle, angiogenesis, DNA repair, cell migration and invasion [15,44-49]. Here, we used a combined gene expression and

proteomic approach to identify candidates of interest through which HDACs were promoting their profound effects on OS metastasis. Our data revealed a number of up and down regulated genes and we focused specifically on NRP1 given its roles in cancer migration and invasion combined with its significant expression in OS clinical cases and correlation with poorer overall survival.

NRP1 was originally identified as a neuronal adhesion molecule but is arguably best studied in the context of vascular biology. NRP1 is anchored to the cell surface with the extracellular portion being comprised of three domains. The FV/VII domain is responsible for the docking of several ligands including vascular endothelial growth factor A (VEGFA), transforming growth factor beta (TGFβ), hepatocyte growth factor (HGF), platelet derived growth factor receptor alpha (PDGFRα) [28]. Additionally, NRP1 binds with ITGB1 to regulate cancer growth, survival and invasion [50]. Previous reports have demonstrated a role for NRP1 in osteosarcoma *in vitro* [30,51]. Our studies agree with these findings but go further and demonstrate a key role for NRP1 in regulating OS lung metastasis *in vivo*. In addition, we also show that activation of SRC, FAK and ROCK1 signaling are the pathways through which NRP1 is promoting OS migration and metastasis. This is, in part, mediated through NRP1/ITGB1 interactions that influence SRC activity. Notably, inhibiting SRC with dasatinib blocked OS migration *in vitro* but had no impact on cell viability as determined by IC_{50} analyses. This suggests that in this model system, SRC contributes more to migration than cell survival. Interestingly, ITBG1 silencing did not completely mirror the effects of NRP1 shRNA on SRC levels. We observed silencing ITGB1 resulted in a greater reduction of SRC phosphorylation compared to the NRP1 shRNA OS cells while conversely, NRP1 shRNA OS cells had lower levels of total SRC. This could be due to temporal effects of siRNA on ITGB1 vs. the stable knockdown of NRP1 or due to additional mechanisms of ITGB1 vs. NRP1 action on SRC. The latter is likely given the abilities of ITGB1 to interact with multiple extracellular matrix proteins and NRP1 to bind receptor tyrosine kinases such as c-MET [52-54]. This may also explain why ITGB1 silencing in control OS cells had little effect on FAK or ROCK1 compared to NRP1 knockdown OS cells. The precise NRP1 binding partner mediating these additional downstream effects remains to be identified and is a focus of future studies by our group.

The K7M2 model of OS is highly aggressive and our results showing that downregulation of NRP1 completely inhibit the lung metastatic potential of the cell line are striking. Our *in vitro* data show that migration and invasion are significantly reduced by NRP1 knockdown but not completely halted. This leads us to hypothesize that in addition to regulating OS migration/invasion, other mechanisms of establishment/engraftment are likely being controlled by NRP1. This is supported, in part, by our orthotopic data showing that NRP1 knockdown also significantly limits the ability of K7M2 to establish to the bone and additionally we have shown in our *in vitro* data, NRP1 knockdown cells have significant decreased cell adhesion capability. The CUB domain of NRP1 is known to bind semaphorin3A, semaphorin4A and plexinA1. These are key mediators of immune and cancer cell transmigration through endothelium such as the blood brain barrier [55,56]. Thus, NRP1 could be an important contributor to OS extravasation from the lung capillary beds into the surrounding parenchyma. Interestingly, NRP1 also plays a key role in immune-evasion by orchestrating inhibitory processes including but not limited to T-cell and

macrophage infiltration into the tumor microenvironment and in suppressing their anti-tumor activity [57]. For robustness, we repeated our lung metastatic studies with the SAOS-LM7 human cell line that requires inoculation into immunocompromised mice. Our findings again show that lung metastasis was significantly abrogated upon knockdown of NRP1. However, unlike the immunocompetent K7M2 model, we did note the presence of micro-metastases in the SAOS-LM7 lungs which may implicate a role for NRP1 in protecting OS cells against immune elimination. Taken together, we posit that NRP1 contributes to OS migration and invasion to the capillary beds in the lung and may play key roles in early extravasation and immunoevasion in this setting.

Our primary purpose in this study was to identify potentially druggable HDAC targets that would not have the potential off-target effects noted with HDAC inhibitors. There have been several strategies to generate NRP1 blocking reagents that range from pharmacological inhibitors to neutralizing antibodies, but none have been successfully translated to the clinic for the treatment of cancer [58]. Despite this, much is known about the downstream effectors of NRP1, particularly regarding cancer cell migration, and these effectors are druggable. For example, blocking SRC prevents OS migration *in vitro* (Fig. 6E). Additionally, clinical trials with inhibitors such as saracatinib (NCT00752206) have been futile for the treatment of lung metastatic OS [59]. This is in keeping with our IC_{50} assay using dasatanib, i.e. no impact on cell viability. This would suggest that the window of treatment for SRC should be at the time of primary cancer detection in order to prevent lung metastases. Defining that window is difficult since 30–40 % OS patients present with metachronous lesions in the lung. But for those that do not display overt disease in the lung, intervention with SRC inhibitors may prove beneficial for preventing or increasing time to lung metastasis [60]. It is also plausible that applying SRC inhibitors in a first strike/second strike manner could be effective strategy for patients presenting with primary OS [61]. In this scenario, the first strike would be traditional MAP chemotherapy to reduce the size and heterogeneity of the OS population. This would then be followed immediately by a second strike with a SRC inhibitor that in turn prevents the potential outgrowth/establishment of lung metastases. Opportunities for targeting downstream effectors such as FAK, ROCK1 and ROCK2 could also potentially be viable approaches as well. Of note, our analysis of the PeCan database of pediatric cancers demonstrated that only ROCK1 and ROCK2 expression was significantly higher in OS patients with concomitantly high NRP1 expression indicating that ROCK1 or ROCK2 inhibition could be more efficacious. Our microarray and proteomic analyses also revealed other potentially targetable HDAC inhibitor-regulated candidates such as matrix metalloproteinase-14 (MMP-14), a peri-cellular type I collagenase and “sheddase” that has known roles in cancer migration, invasion and metastasis [62]. However, clinical trials with broad and selective MMP inhibitors were largely unsuccessful and enthusiasm for further development has been lacking. Other interesting HDACi targets include solute carrier family 17 member 7 (SLC17A7) which is a key regulator of cellular glutamine levels. OS is heavily reliant on glutamine metabolism for growth and induction of oncogenic programs driven by MYC [63]. Our data show that HDAC inhibition upregulates SLC17A7 which in turn helps with cellular export of glutamine [64]. Emerging studies have shown that targeting the enzymes that control glutamine metabolism can be an effective means with which to limit OS growth in preclinical animal models [65]. Therefore, targeting this metabolic

vulnerability could prove useful for the treatment of OS in the primary and/or metastatic setting.

In summary, our data has shown that HDACs control the expression of a number of target genes that are implicated in cancer progression. Here we focused particularly on NRP1 whose expression in OS cells was significantly downregulated in response to treatment with the HDAC 1 and 2 inhibitor, romidepsin. Our results show that reducing NRP1 expression significantly inhibited OS migration and invasion *in vitro* and dramatically limited the ability of OS cells to successfully seed the lung and establish metastases *in vivo*. Mechanistically, this is in part due to NRP1 controlling the activity and signaling of key molecules with known functions in cancer cell migration such as SRC, FAK, ROCK1 and ROCK2 via the binding of ITGB1 and likely other receptor tyrosine kinases. Taken together, our result indicates that targeting either NRP1 or its downstream effectors would be effective in limiting OS lung metastasis, particularly for patients who present with no evidence of metachronous disease. Our data also identifies other targets of HDAC inhibitors whose specific inhibition may prove useful for OS treatment.

4. Methods

4.1. Cell lines

SAOS-LM7 (RRID:CVCL_0515) were a kind gift from Dr Eugenie Kleinerman, MD Anderson, MG63(RRID:CVCL_0426), SAOS2(RRID: CVCL_0548) from ATCC and K7M2 (RRID: CVCL_V455) were a kind gift from Dr Chand Khanna, NCI. All cell lines were periodically tested and determined to be mycoplasma free (R&D Systems, Minneapolis, Minnesota, Cat#: CUL001B). All human cell lines were validated by short tandem repeat (STR Moffitt genomics core) and mouse cell lines via IDEXX BioAnalytics within the last 6 months. All cell lines were passaged in DMEM culture medium supplemented with 10% fetal bovine serum and 1% penicillin and streptomycin antibiotic.

4.2. qRT-PCR, immunoblotting and phospho-kinase array

Cells were washed with 1X PBS before extracting total RNA using TRIzol (Invitrogen, Carlsbad, California, Cat#:15596026) as per manufacturer’s instruction. Nanodrop was used to quantify RNA quantity. cDNA was generated using High-Capacity cDNA Reverse Transcription Kit (Applied Biosystems, Foster City, California, Cat#: 4368813), 1 μg of total RNA was used per sample. Human and mouse primers for validation of microarray analysis and downstream genes involved in downstream mechanism of NRP1 were synthesized from Integrated DNA Technologies (IDT DNA). All primer sequences are listed in Table S1. To quantify gene expression using qRT-PCR, SYBR Green reagent (Applied Biosystems, Foster City, California, Cat#: 4309155) was used and reaction were performed using Quant Studio 5 Real-Time PCR System (Applied Biosystems). Actin was used as an internal control to normalize across samples.

For immunoblotting, cells were washed twice with chilled 1X phosphate buffer saline (PBS), followed by lysis with RIPA buffer (150 mM NaCl, 1 mM EDTA, 1% Triton X-100, 1% sodium deoxycholate, 0.1% SDS, 20 mM Tris, pH 8) containing HALT protease

inhibitor cocktail (Thermo Fisher Scientific, Waltham, Massachusetts, Cat#: 78442) to extract proteins. Total protein was quantified using BCA (Pierce, Waltham, Massachusetts, Cat#: 23225) assay as per manufacturer's instruction. Different concentrations of Tris gels were used depending on the molecular weight of the protein. Nitrocellulose membrane (Biorad, Hercules, California, Cat#:1620211) was used to transfer the proteins from gel. Upon transfer, blots were blocked in 5% bovine serum albumin (BSA) for 1 h followed by overnight primary antibody incubation at 1:1000 dilution in blocking solution containing 0.1% Tween 20 placed at 4 °C on a rocker. Blots were washed thrice with 1X Tris-buffered saline with 0.5% Tween 20 (TBST) for 10 min each and then incubated with HRP-conjugated anti-species secondary respective of each primary antibody for 1 h at 1:1000 dilution in blocking solution containing 0.1% Tween-20 placed at room temperature on a rocker. Catalog numbers for all primary and secondary antibodies are listed in Table S2. Blots were washed thrice with 1X TBST for 10 min each and then chemiluminescent (ECL) substrate (Thermo Fisher Scientific, Waltham, Massachusetts, Cat#: 32016) is added to blots to detect HRP tagged proteins using LI-COR Odyssey Fc imager. Protein bands were quantified using LI-COR image studio software. Actin and Vinculin were used as internal control to normalize the proteins across samples. For immunoblot in Fig. 6C, cells were serum starved for 24h, followed by addition of DMEM media with 10% serum for 5 min, 15 min and 1-h timepoints. For immunoblot in Fig. 6F, cells were transfected with control or ITGB1 siRNA, after 72h protein lysates were collected to analyze protein expression.

For phospho-kinase array analysis, cell lysates from control or NRP1 knockdown cells were collected according to manufacturer's instructions. Phospho-kinase array blotting using Proteome Profiler Human Phospho-Kinase Array Kit was performed with cell lysates as per kit instructions (R&D Biosystems, Minneapolis, Minnesota, Cat#: ARY003C) and detected using Odyssey Fc Imaging System (LI-COR).

4.3. siRNA and shRNA constructs

For *NRP1* and *ITGB1* silencing, NRP1, ITGB1 and Control siRNA were purchased from Horizon Discovery (Cat#: L-040787-00-0005, L-040783-01-0005 and D-001810-01-05, respectively). Seed 1.0×10^5 K7M2 or SAOS-LM7 cells per each well of 6-well plate. To prepare siRNA master mix, add 5ul of Lipofectamine RNAiMAX(Cat#: 13778030) solution and 9ul of 10 nM siRNA solution to 500ul of Opti-MEM media for transfecting each well of 6-well of plates. Vortex the mix for 5 s and then incubate the mix for 20 min at room temperature. Meanwhile, wash the cells with 1x PBS, followed by addition of fresh 500ul of Opti-mem media per well. After 20 min, add siRNA master mix to respective wells. After 6h, add pen-strep free complete DMEM media to wells. Cells are collected at different timepoints. For immunoblot in Fig. 6F, seed 1.0×10^5 control and NRP1 shRNA K7M2 cells per each well of 6-well plate. Next day, transfect cells with Control and ITGB1 siRNA as mentioned above. After 72h of incubation, protein lysates were collected for immunoblot.

Additionally, shRNA constructs were purchased from Horizon Discovery. Stable *NRP1* knockdown cell lines were generated using TRC Lentiviral Mouse Nrp1 shRNA constructs (Cat#: RMM4534-EG18186) and TRC Lentiviral Human NRP1 shRNA constructs (Cat#: RHS4533-EG8829). HEK293T cells were used to generate viral particles. To perform

transfection, 5ul of FuGENE® 6 Transfection Reagent (Promega, Madison, Wisconsin, Cat #E2693) was used according to manufacturer's instruction. After 48h of transfection, positive clones were selected using puromycin. Clones were established by seeding 1 cell per well of 96 well plate and let them grow till confluence reached in 96 well plate. Then the clones were transferred to different size plates until they reached confluence in 6 well plate, they were divided into two wells. One well of cells were used to collect RNA and confirm NRP1 knockdown using qRT-PCR and other well of cells were used to expand the clones.

4.4. In vivo studies

All mice (BALB/c and NSG) aged six weeks old were purchased from Jackson Laboratories (Bar Harbor, Maine, USA) and before initiating experiments were maintained for at least 5 days in pathogen free conditions in the animal facility as per the guidelines and standards of the American Association of Accreditation of Laboratory Animal Care (AAALAC). All animal experiments were conducted in compliance with relevant ethical regulations and protocols and approved by the Institutional Animal Care and Use Committee (IACUC) at the University of South Florida under protocols IS00007896R (approved on 5/4/20) and IS00011705R (approved on 2/24/23). For established lung metastasis studies, 1.0×10^6 control and NRP1 shRNA K7M2 cells and 1.5×10^6 control and NRP1 shRNA SAOS-LM7 cells were injected via tail vein into female BALB/c or female NSG mice, respectively. For primary orthotopic bone studies, 1.0×10^5 control and NRP1 shRNA K7M2 cells were injected intratibially in 20 μL of sterile PBS into one of the tibia of female BALB/c mice. As a control, the contralateral tibia was injected with 20 μL of sterile PBS. Mice weights were recorded five days per week for the duration of the study.

4.5. Ex vivo lung analysis

At the study endpoint, lungs were perfused, inflated, and fixed with Bouin's fixative solution. Collected lungs were then incubated in 10% formalin for 24 h at room temperature and transferred to 70% ethanol solution. Prior to paraffin embedding, lung macro-metastases on the lungs were counted manually with naked eye. Paraffin embedded lungs were sectioned at 5 μM thickness for hematoxylin and eosin (H&E) staining. H&E staining (Millipore Sigma, Burlington, Massachusetts, Cat#: MHS16) was performed as per manufacturer's instructions. Sections were scanned at 20X using microscopy. ImageJ software was used to quantify tumor area and total area of lung section.

4.6. Ex vivo bone analysis

Collected tibias were fixed in 10% formalin for 24 h and then transferred to 70% ethanol solution. Tibias were decalcified using 14% EDTA, pH 7.4, for 3 weeks. Tibias were then paraffin-embedded and sectioned at 5 μM thickness. H&E staining was performed to assess tumor burden.

4.7. Cell migration and invasion assay

Cells were seeded at 1×10^6 cells per 10 cm dish. Next day, cells were washed with 1X PBS and media replaced with serum free for 24 h. After trypsinization, cells were counted and seeded 100,000 cells in 250 μL serum free media in the upper chamber of transwell

insert. In the lower chamber, 650 μL of 1% serum media is added. Cells were fixed after 3 h and 7 h for SAOS-LM7 and K7M2 cells, respectively, in chilled 100% methanol for 5 min. Unmigrated cells in the upper chamber were removed by scrubbing with a cotton swab. Inserts were fixed in hematoxylin for 8 min to stain migrated cells, followed by 30 s in 1X PBS and then placed in 100% ethanol for 30 s for drying. Dried membranes containing migrated cells were excised using a scalpel and mounted on glass slides with permount. Four 20X magnification fields were captured per group. Image J software was used to count the cells. For invasion assay, Matrigel coated plates were used (Corning, Corning, New York, Cat#:354480). After seeding(5×10^4 cells), cells were incubated for 24 h in transwell inserts to perform the invasion assay.

4.8. In silico data analysis

SAOS2 and MG63 cells were treated with romidepsin for 24 h and collected to extract RNA. RNA was hybridized to Affymetrix U133 Plus 2.0 GeneChip microarrays (Affymetrix, Inc., Santa Clara, CA). Using R, expression levels were normalized by GCRMA. To identify significantly differentially expressed genes, log fold change of less than −1 for downregulated genes and log fold change greater than 1 for upregulated genes with adjusted P value of less than 0.05 was chosen as cut-off. For proteomic analysis, romidepsin treated group values were normalized with respective control group values to identify fold change per protein. For pathway enrichment analysis, EnrichR (https://maayanlab.cloud/Enrichr/) was used to identify differentiated biological processes.

For RNASeq analyses of target genes in patient data, we availed of the publicly available dataset generated by St. Jude Children's Hospital (Memphis, TN, USA (https://pecan.stjude.cloud/); [38]. All patient information is deidentified for users and thus considered non-human subject research. Fragments Per Kilobase per Million mapped fragments (FPKM) values for respective genes were downloaded for each patient. There was total of 2486 samples for all pediatric cancers, from which 109 were osteosarcoma patients. For Fig. 1 analysis, samples were divided into other (non-osteosarcoma) and OS (osteosarcoma) samples. For Fig. 6 analysis, osteosarcoma patient samples were divided into two groups based on NRP1 expression. Top 35 NRP1 expressing samples were considered as NRP1 high and low 35 NRP1 expressing samples as NRP1 low groups from total 109 patient samples. Based on these two groups, FPKM values for other genes were segregated.

4.9. Cytotoxicity and cell proliferation assays

Control and NRP1 shRNA K7M2 cells were seeded at 2000 cells per well in a white bottom 96-well plates in triplicate. After 24 h, cells were treated with dasatinib and romidepsin at the following dosages: 0, 7.81, 15.62, 31.25, 62.5, 125, 250, 500, 1000, 2000 nM. After 24 and 48 h, 20 μL of CellTiter-Glo® One Solution Assay (Promega, Madison, Wisconsin, Cat#: G8461) was added to wells. Plates were wrapped with aluminum foil and incubated for 10 min at room temperature before reading the luminescence using BioTek plate reader. IC_{50} values were determined using GraphPad Prism 10.0 software.

For cell proliferation assays, control or knockdown/silenced cells were seeded at 2000 cells per each well of 96-well plate in triplicate for each group in 3 plates. At 24, 48 and 72 h,

luminescence reading was performed using 20 μL of CellTiter-Glo® One Solution Assay. Luminescence measurements were normalized to respective 24 h timepoints.

4.10. Cell adhesion assay

Seed 1.5×10^6 control and NRP1 shRNA K7M2 cells in a 10 cm plate. Next day, wash the cells with 5 ml of 1x PBS and then trypsinize the cells with 2 ml of 0.25% trypsin at 37 °C. After 5 min, resuspend two replicates of 4×10^5 cells/ml control and NRP1 shRNA K7M2 cells in serum free DMEM media containing 1% BSA each. While one replicate of cells is incubated with 5ug/ml Armenian Hamster IgG Isotype Control (eBio299Arm, Thermo Fisher Scientific, Waltham, Massachusetts, catalog# 16-4888-85) and other replicate of cells is incubated with 5ug/ml CD29 (Integrin beta 1) Monoclonal Antibody (eBioHMb1-1 (HMb1-1, Thermo Fisher Scientific, Waltham, Massachusetts, catalog# 16-029185)) for 60 min at 37 ° C. In the meanwhile, fibronectin coated 96 wells plates (Fisher scientific, Hampton, New Hampshire, catalog# 08774-60) is washed with 100ul of wash buffer (serum free DMEM media containing 0.1% BSA) per well. Then add, 50ul of blocking buffer (DMEM serum free media containing 0.5% BSA) to each well of fibronectin coated plates and then incubate at 37 °C. After 45 min, wash the plates twice with 100ul/well wash buffer. Followed by addition of 50ul per well (3 wells each) of control and NRP1 shRNA K7M2 cells neutralized with IgG/Integrin beta 1 antibody to assess cell adhesion. Incubate the plate at 37 ° C in the incubator, followed by capturing three 20X images per well of 96 well plate with Evos light microscope. Adherent and non-adherent (round cells) were counted per image using imageJ and then normalized with total cells per image.

4.11. Statistical analysis

GraphPad Prism 10.0 (GraphPad Inc., La Jolla, California) was used to perform all statistical analysis. To determine statistical significance, T-test was performed for 2 groups and 2-way ANOVA test was performed for multiple comparisons. P-value of less than 0.05 was considered significant. All data included standard errors of mean (SEM).

Supplementary Material

Refer to Web version on PubMed Central for supplementary material.

Acknowledgements

The authors would like to thank Dr. Jeremy Frieling at the Moffitt Cancer Center for critical review of this work. This work has been financially supported in part by the Live Like Bella Pediatric Cancer Research Initiative, Florida Department of Health (23L09 CCL), Chotiner foundation (CCL), the H. Lee Moffitt Cancer Center & Research Institute Adolescent and Young Adult program and by the shared resources at the Moffitt Cancer Center, an NCI designated Comprehensive Cancer Center (P30-CA076292).

References

[1]. Mirabello L, Troisi RJ, Savage SA, Osteosarcoma incidence and survival rates from 1973 to 2004: data from the surveillance, epidemiology, and end results program, Cancer: Interdisciplin. Int. J. Am. Cancer Soc 115 (7) (2009) 1531–1543.

[2]. Bacci G, et al. , High grade osteosarcoma of the extremities with lung metastases at presentation: treatment with neoadjuvant chemotherapy and simultaneous resection of primary and metastatic lesions, J. Surg. Oncol 98 (6) (2008) 415–420. [PubMed: 18792969]

[3]. Bielack SS, et al. , Second and subsequent recurrences of osteosarcoma: presentation, treatment, and outcomes of 249 consecutive cooperative osteosarcoma study group patients, J. Clin. Oncol 27 (4) (2009) 557–565. [PubMed: 19075282]

[4]. Meazza C, Scanagatta P, Metastatic osteosarcoma: a challenging multidisciplinary treatment, Expet Rev. Anticancer Ther 16 (5) (2016) 543–556.

[5]. Link MP, et al. , The effect of adjuvant chemotherapy on relapse-free survival in patients with osteosarcoma of the extremity, N. Engl. J. Med 314 (25) (1986) 1600–1606. [PubMed: 3520317]

[6]. Smeland S, et al. , Survival and prognosis with osteosarcoma: outcomes in more than 2000 patients in the EURAMOS-1 (European and American Osteosarcoma Study) cohort, Eur. J. Cancer 109 (2019) 36–50. [PubMed: 30685685]

[7]. Kager L, et al. , Primary metastatic osteosarcoma: presentation and outcome of patients treated on neoadjuvant Cooperative Osteosarcoma Study Group protocols, J. Clin. Oncol 21 (10) (2003) 2011–2018. [PubMed: 12743156]

[8]. Isakoff MS, et al. , Rapid protocol enrollment in osteosarcoma: a report from the Children's Oncology Group, Pediatr. Blood Cancer 63 (2) (2016) 370. [PubMed: 26376351]

[9]. Lizardo MM, et al. , Abstract A024: a potent eIF4A1/2 inhibitor CR-1-31B down-modulates the antioxidant stress response in osteosarcoma cells and inhibits in vivo lung metastases, Cancer Res. 83 (2_Supplement_2) (2023). A024–A024.

[10]. Cripe TP, et al. , Progress in sarcomas: highlights from the 2023 annual meetingof the connective tissue oncology society, Molecul. Ther. Oncol 32 (1) (2024).

[11]. McAloney CA, et al. , Host-derived growth factors drive ERK phosphorylation and MCL1 expression to promote osteosarcoma cell survival during metastatic lung colonization, Cell. Oncol 47 (1) (2024) 259–282.

[12]. Morrow JJ, et al. , Positively selected enhancer elements endow osteosarcoma cells with metastatic competence, Nat. Med 24 (2) (2018) 176–185. [PubMed: 29334376]

[13]. Rajan S, et al. , Osteosarcoma tumors maintain intra-tumoral transcriptional heterogeneity during bone and lung colonization, BMC Biol. 21 (1) (2023) 98. [PubMed: 37106386]

[14]. Yu D, et al. , Identification of synergistic, clinically achievable, combination therapies for osteosarcoma, Sci. Rep 5 (1) (2015) 16991. [PubMed: 26601688]

[15]. McGuire JJ, et al. , Histone deacetylase inhibition prevents the growth of primary and metastatic osteosarcoma, Int. J. Cancer 147 (10) (2020) 2811–2823. [PubMed: 32599665]

[16]. Bailey H, Stenehjem DD, Sharma S, Panobinostat for the treatment of multiple myeloma: the evidence to date, Hematol. Res. Rev (2015) 269–276.

[17]. Sivaraj D, Green MM, Gasparetto C, Panobinostat for the management of multiple myeloma, Future Oncol. 13 (6) (2017) 477–488. [PubMed: 27776419]

[18]. Smolewski P, Robak T, The discovery and development of romidepsin for the treatment of T-cell lymphoma, Expet Opin. Drug Discov 12 (8) (2017) 859–873.

[19]. Kolodkin AL, et al. , Neuropilin is a semaphorin III receptor, Cell 90 (4) (1997) 753–762. [PubMed: 9288754]

[20]. Nakamura F, et al. , Neuropilin-1 extracellular domains mediate semaphorin D/III-induced growth cone collapse, Neuron 21 (5) (1998) 1093–1100. [PubMed: 9856464]

[21]. Soker S, et al. , Neuropilin-1 is expressed by endothelial and tumor cells as an isoform-specific receptor for vascular endothelial growth factor, Cell 92 (6) (1998) 735–745. [PubMed: 9529250]

[22]. Achen MG, Stacker SA, The vascular endothelial growth factor family; proteins which guide the development of the vasculature, Int. J. Exp. Pathol 79 (5) (1998) 255–265. [PubMed: 10193309]

[23]. Li L, et al. , Neuropilin-1 is associated with clinicopathology of gastric cancer and contributes to cell proliferation and migration as multifunctional co-receptors, J. Exp. Clin. Cancer Res 35 (2016) 1–12. [PubMed: 26728266]

[24]. Rizzolio S, et al. , Neuropilin-1–dependent regulation of EGF-receptor signaling, Cancer Res. 72 (22) (2012) 5801–5811. [PubMed: 22986738]

[25]. West DC, et al. , Interactions of multiple heparin binding growth factors with neuropilin-1 and potentiation of the activity of fibroblast growth factor-2, J. Biol. Chem 280 (14) (2005) 13457–13464. [PubMed: 15695515]

[26]. Yoshida A, et al. , VEGF-A/NRP1 stimulates GIPC1 and Syx complex formation to promote RhoA activation and proliferation in skin cancer cells, Biol. open 4 (9) (2015) 1063–1076. [PubMed: 26209534]

[27]. Valdembri D, et al. , Neuropilin-1/GIPC1 signaling regulates α5β1 integrin traffic and function in endothelial cells, PLoS Biol. 7 (1) (2009) e1000025. [PubMed: 19175293]

[28]. Niland S, Eble JA, Neuropilins in the context of tumor vasculature, Int. J. Mol. Sci 20 (3) (2019) 639. [PubMed: 30717262]

[29]. Cruz da Silva E, et al. , Role of integrins in resistance to therapies targeting growth factor receptors in cancer, Cancers 11 (5) (2019) 692. [PubMed: 31109009]

[30]. Zhu H, et al. , Neuropilin-1 is overexpressed in osteosarcoma and contributes to tumor progression and poor prognosis, Clin. Transl. Oncol 16 (2014) 732–738. [PubMed: 24338507]

[31]. Hong T-M, et al. , Targeting neuropilin 1 as an antitumor strategy in lung cancer, Clin. Cancer Res 13 (16) (2007) 4759–4768. [PubMed: 17699853]

[32]. Ma X, et al. , Bioinformatics analysis and clinical significance of NRP-1 in triple-negative breast cancer, Heliyon 10 (5) (2024) e27368. [PubMed: 38495206]

[33]. Ben Q, et al. , High neuropilin 1 expression was associated with angiogenesis and poor overall survival in resected pancreatic ductal adenocarcinoma, Pancreas 43 (5) (2014) 744–749. [PubMed: 24632553]

[34]. Huang Z, et al. , NRP1 promotes cell migration and invasion and serves as a therapeutic target in nasopharyngeal carcinoma, Int. J. Clin. Exp. Pathol 11 (5) (2018) 2460. [PubMed: 31938358]

[35]. Jin Q, et al. , Neuropilin-1 predicts poor prognosis and promotes tumor metastasis through epithelial-mesenchymal transition in gastric cancer, J. Cancer 12 (12) (2021) 3648. [PubMed: 33995640]

[36]. Jimenez-Hernandez LE, et al. , NRP1-positive lung cancer cells possess tumor-initiating properties, Oncol. Rep 39 (1) (2018) 349–357. [PubMed: 29138851]

[37]. Kimura H, et al. , Imaging the inhibition by anti-β1 integrin antibody of lung seeding of single osteosarcoma cells in live mice, Int. J. Cancer 131 (9) (2012) 2027–2033. [PubMed: 22323248]

[38]. McLeod C, et al. , St. Jude Cloud: a pediatric cancer genomic data-sharing ecosystem, Cancer Discov. 11 (5) (2021) 1082–1099. [PubMed: 33408242]

[39]. Li R, et al. , NF-κB signaling and integrin-β1 inhibition attenuates osteosarcoma metastasis via increased cell apoptosis, Int. J. Biol. Macromol 123 (2019) 1035–1043. [PubMed: 30399378]

[40]. Bielack SS, et al. , Osteosarcoma and causes of death: a report of 1520 deceased patients from the Cooperative Osteosarcoma Study Group (COSS), Eur. J. Cancer 176 (2022) 50–57. [PubMed: 36191386]

[41]. Schuetze SM, et al. , SARC009: phase 2 study of dasatinib in patients with previously treated, high-grade, advanced sarcoma, Cancer 122 (6) (2016) 868–874. [PubMed: 26710211]

[42]. Jurkin J, et al. , Distinct and redundant functions of histone deacetylases HDAC1 and HDAC2 in proliferation and tumorigenesis, Cell Cycle 10 (3) (2011) 406–412. [PubMed: 21270520]

[43]. Ramaiah MJ, Tangutur AD, Manyam RR, Epigenetic modulation and understanding of HDAC inhibitors in cancer therapy, Life Sci 277 (2021) 119504. [PubMed: 33872660]

[44]. Li Y, Seto E, HDACs and HDAC inhibitors in cancer development and therapy, Cold Spring Harbor Perspect. Med 6 (10) (2016) a026831.

[45]. Bhaskara S, et al. , Deletion of histone deacetylase 3 reveals critical roles in S phase progression and DNA damage control, Mol. Cell 30 (1) (2008) 61–72. [PubMed: 18406327]

[46]. Li G, Tian Y, Zhu W-G, The roles of histone deacetylases and their inhibitors in cancer therapy, Front. Cell Dev. Biol 8 (2020) 576946. [PubMed: 33117804]

[47]. Hai R, et al. , Characterization of histone deacetylase mechanisms in cancer development, Front. Oncol 11 (2021) 700947. [PubMed: 34395273]

[48]. Xu L, et al. , Suppression of histone deacetylase 1 by JSL-1 attenuates the progression and metastasis of cholangiocarcinoma via the TPX2/Snail axis, Cell Death Dis. 13 (4) (2022) 324. [PubMed: 35395834]

[49]. Zheng L, et al. , HDAC1 promotes the migration of human myeloma cells via regulation of the lncRNA/Slug axis, Int. J. Mol. Med 49 (1) (2022) 1–9. [PubMed: 34713301]

[50]. Fukasawa M, Matsushita A, Korc M, Neuropilin-1 interacts with integrin β1 and modulates pancreatic cancer cell growth, survival and invasion, Cancer Biol. Ther 6 (8) (2007) 1184–1191.

[51]. Yue B, et al. , Knockdown of neuropilin-1 suppresses invasion, angiogenesis, and increases the chemosensitivity to doxorubicin in osteosarcoma cells–an in vitro study, Eur. Rev. Med. Pharmacol. Sci 18 (12) (2014).

[52]. Matsushita A, Götze T, Korc M, Hepatocyte growth factor–mediated cell invasion in pancreatic cancer cells is dependent on Neuropilin-1, Cancer Res. 67 (21) (2007) 10309–10316. [PubMed: 17974973]

[53]. Bredin C, et al. , Integrin dependent migration of lung cancer cells to extracellular matrix components, Eur. Respir. J 11 (2) (1998) 400–407. [PubMed: 9551745]

[54]. Jahangiri A, et al. , Cross-activating c-Met/β1 integrin complex drives metastasis and invasive resistance in cancer, Proc. Natl. Acad. Sci. USA 114 (41) (2017) E8685–E8694. [PubMed: 28973887]

[55]. Nakamura F, Goshima Y, Structural and functional relation of neuropilins, Neuropilin: From Nervous Syst. Vascul. Tumor Biol (2002) 55–69.

[56]. Klotz R, et al. , Circulating tumor cells exhibit metastatic tropism and reveal brain metastasis drivers, Cancer Discov. 10 (1) (2020) 86–103. [PubMed: 31601552]

[57]. Chuckran CA, et al. , Neuropilin-1: a checkpoint target with unique implications for cancer immunology and immunotherapy, J. Immun.Ther. Cancer 8 (2) (2020) e000967.

[58]. Liu S-D, et al. , Targeting neuropilin-1 interactions is a promising anti-tumor strategy, Chinese Med J 134 (5) (2021) 508–517.

[59]. Baird K, et al. , Results of a randomized, double-blinded, placebo-controlled, phase 2.5 study of saracatinib (AZD0530), in patients with recurrent osteosarcoma localized to the lung, Sarcoma (2020) 2020.

[60]. Gok Durnali A, et al. , Outcomes of adolescent and adult patients with lung metastatic osteosarcoma and comparison of synchronous and metachronous lung metastatic groups, PLoS One 11 (5) (2016) e0152621. [PubMed: 27167624]

[61]. Reed DR, et al. , An evolutionary framework for treating pediatric sarcomas, Cancer 126 (11) (2020) 2577–2587. [PubMed: 32176331]

[62]. Gonzalez-Molina J, et al. , MMP14 in sarcoma: a regulator of tumor microenvironment communication in connective tissues, Cells 8 (9) (2019) 991. [PubMed: 31466240]

[63]. Anso E, et al. , Metabolic changes in cancer cells upon suppression of MYC, Cancer Metabol. 1 (2013) 1–10.

[64]. Nerlakanti N, et al. , Delineating the role of vesicular glutamate transporter SLC17A7 in osteosarcoma, Cancer Res. 83 (7_Supplement) (2023), 276–276.

[65]. Ren L, et al. , Glutaminase-1 (GLS1) inhibition limits metastatic progression in osteosarcoma, Cancer Metabol. 8 (2020) 1–13.

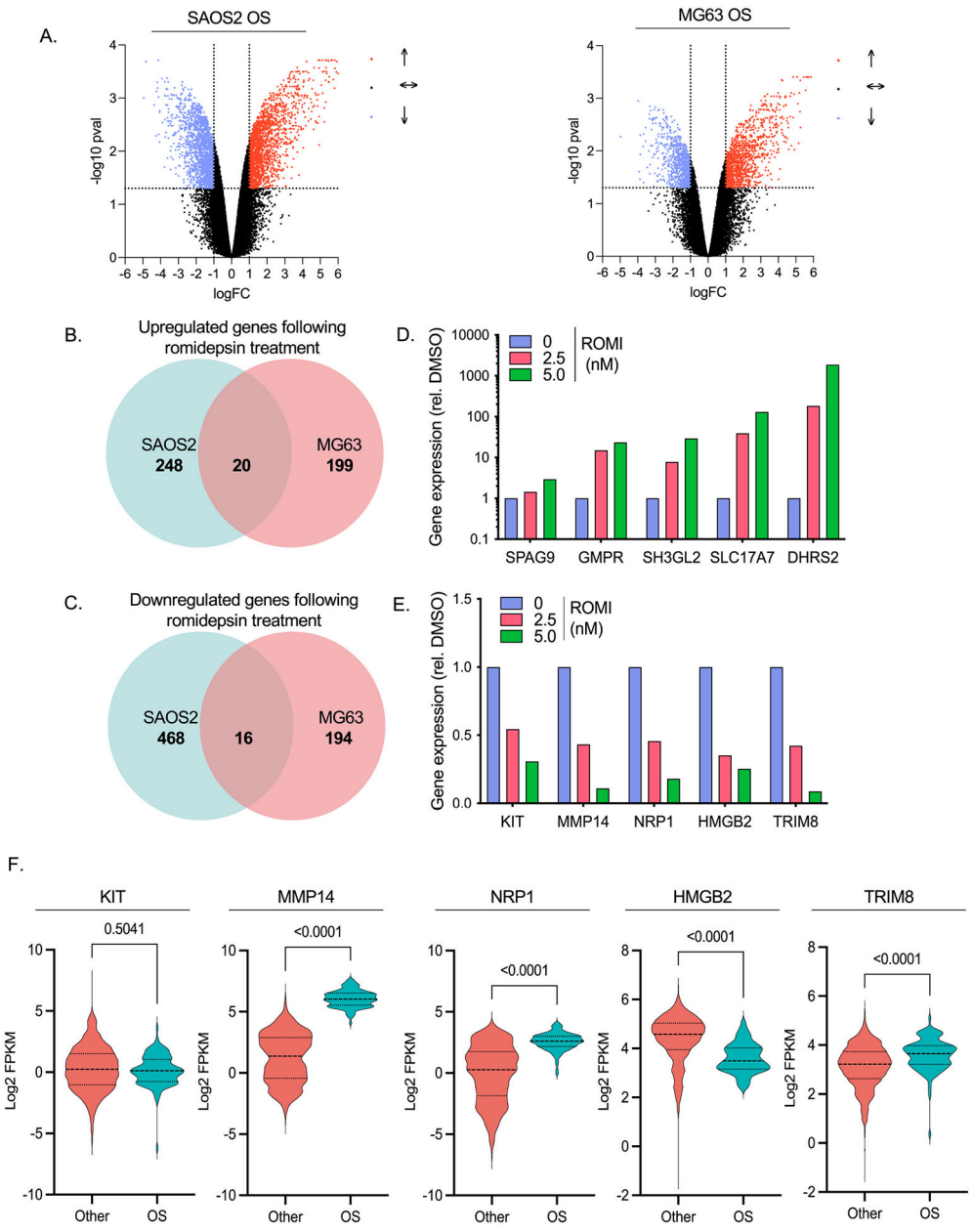

Fig. 1. Effect of romidepsin on genome-wide transcription in osteosarcoma.

A. Volcano plots showing differentially expressed genes analyzed after romidepsin treatment in SAOS2 and MG63 cell lines; pval means adjusted p value and FC means fold change in gene expression; red dots are indicating significant upregulated genes and blue dots are indicating significant downregulated genes and black dots are indicating insignificant genes. B,C. Venn diagram showing common upregulated and downregulated genes between SAOS2 and MG63 genes respectively. D,E. *In vitro* validation of upregulated and downregulated genes after 24h romidepsin (ROMI) treatment in SAOS-LM7 cell line using qRT-PCR respectively. F. RNA-seq data from St. Jude PeCan database was used to compare Fragments Per Kilobase of transcript per Million mapped reads (FPKM) between other pediatric cancer patients (Other) vs Osteosarcoma patients (OS) for downregulated genes.

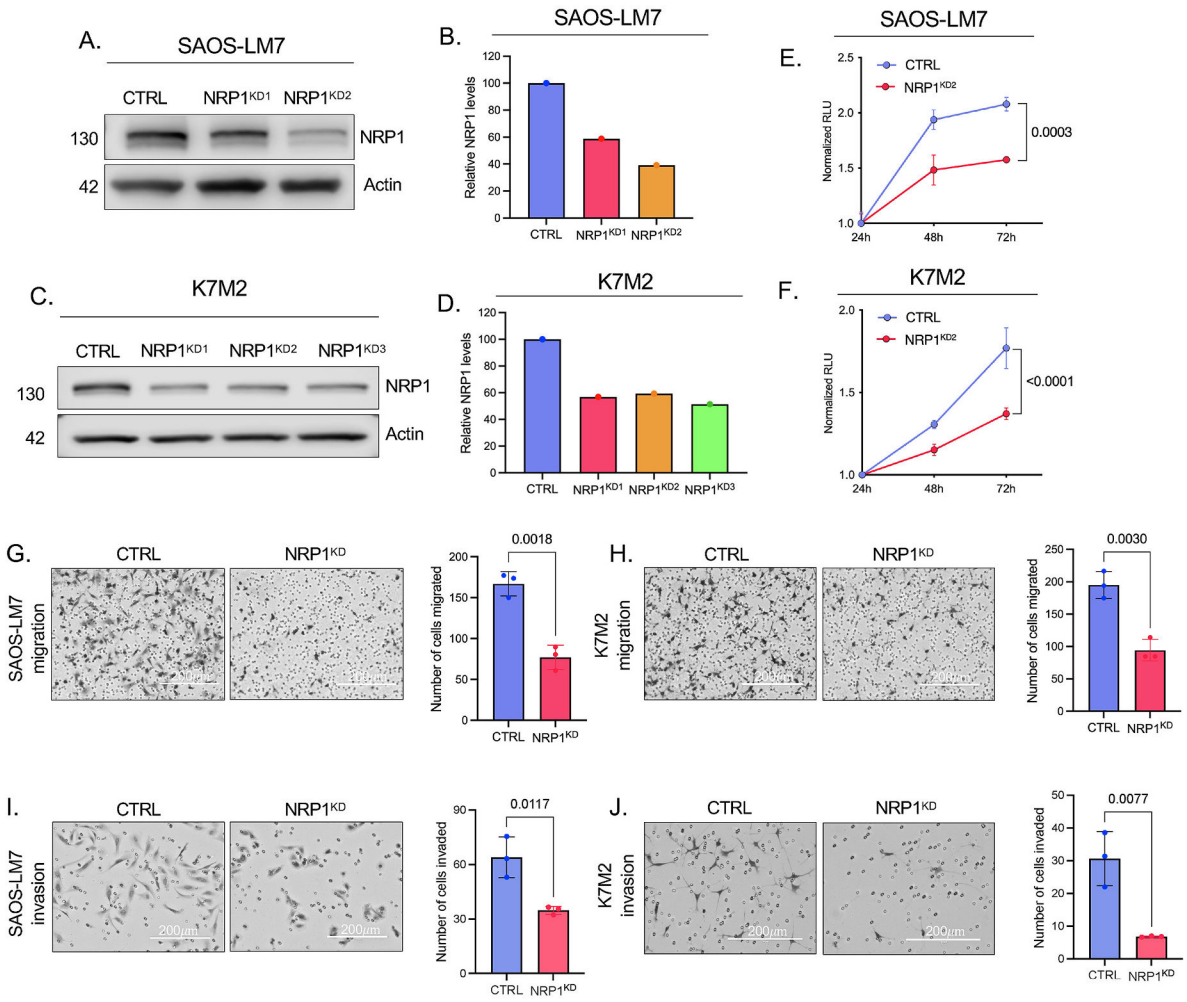

Fig. 2. Constitutive downregulation of NRP1 contribute to osteosarcoma growth inhibition.

A,C. Immunoblots shows downregulation of NRP1 levels in NRP1 shRNA generated clones of SAOS-LM7 and K7M2 NRP1 cell lines respectively. B,D. Immunoblot quantification of A,C blots showing downregulation of NRP1 protein levels in SAOS-LM7 and K7M2 NRP1 shRNA clones respectively. Actin was used as a positive loading control. E,F. Analysis of cell proliferation rates between control and NRP1 shRNA groups for SAOS-LM7 and K7M2 cells respectively at 24h, 48h and 72h timepoints. RLU denotes relative luminescence units. G, H. Hematoxylin-stained images of migrated cells and it's quantification in control and NRP1 shRNA groups for SAOS-LM7 and K7M2 cells respectively. I, J. Hematoxylin-stained images of invaded cells and its quantification in control and NRP1 shRNA groups for SAOS-LM7 and K7M2 cells respectively. CTRL denotes Control shRNA and $NRP1^{KD}$ denotes NRP1 shRNA.

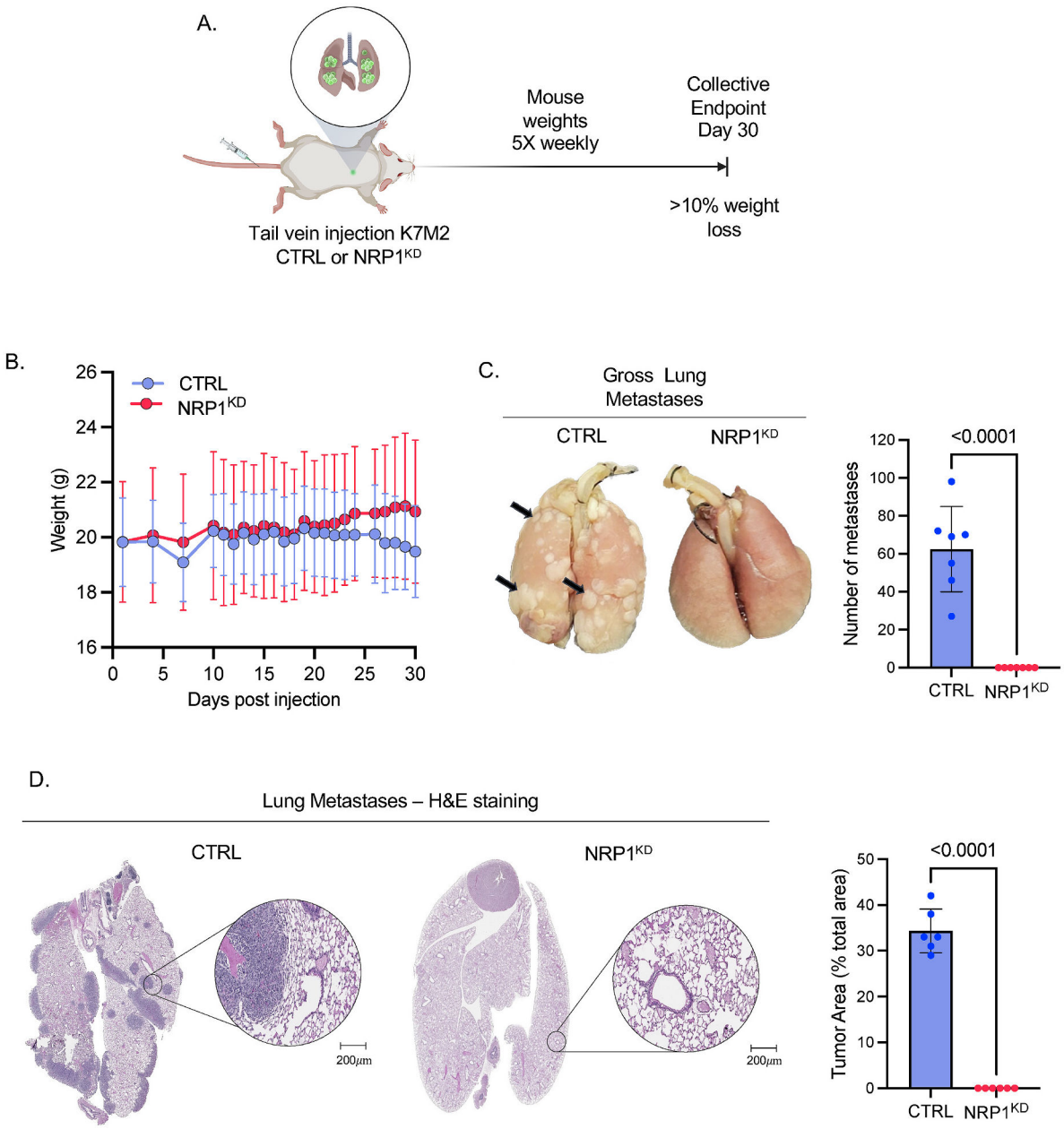

Fig. 3. Neuropilin-1(NRP1) knockdown inhibits established osteosarcoma lung metastasis.

A. Experimental design: K7M2 control shRNA and NRP1 shRNA cells were tail vein inoculated into immunocompetent BALB/c mice, mice were weighted five times per week and collective endpoint of the study was Day 30. B. Weight of the mice (grams) injected with K7M2 control shRNA and NRP1 shRNA cells. C. At the endpoint, lungs from each group were inflated with Bouin's fixative solution and the number of surface metastases(mets; black arrows) were counted. Black arrows indicate surface metastases. D. Lung sections were stained with hematoxylin and eosin to analyze the percent tumor volume compared to total volume of lungs section using ImageJ. Inset scale bar = 200 μm. CTRL denotes Control shRNA and $NRP1^{KD}$ denotes NRP1 shRNA.

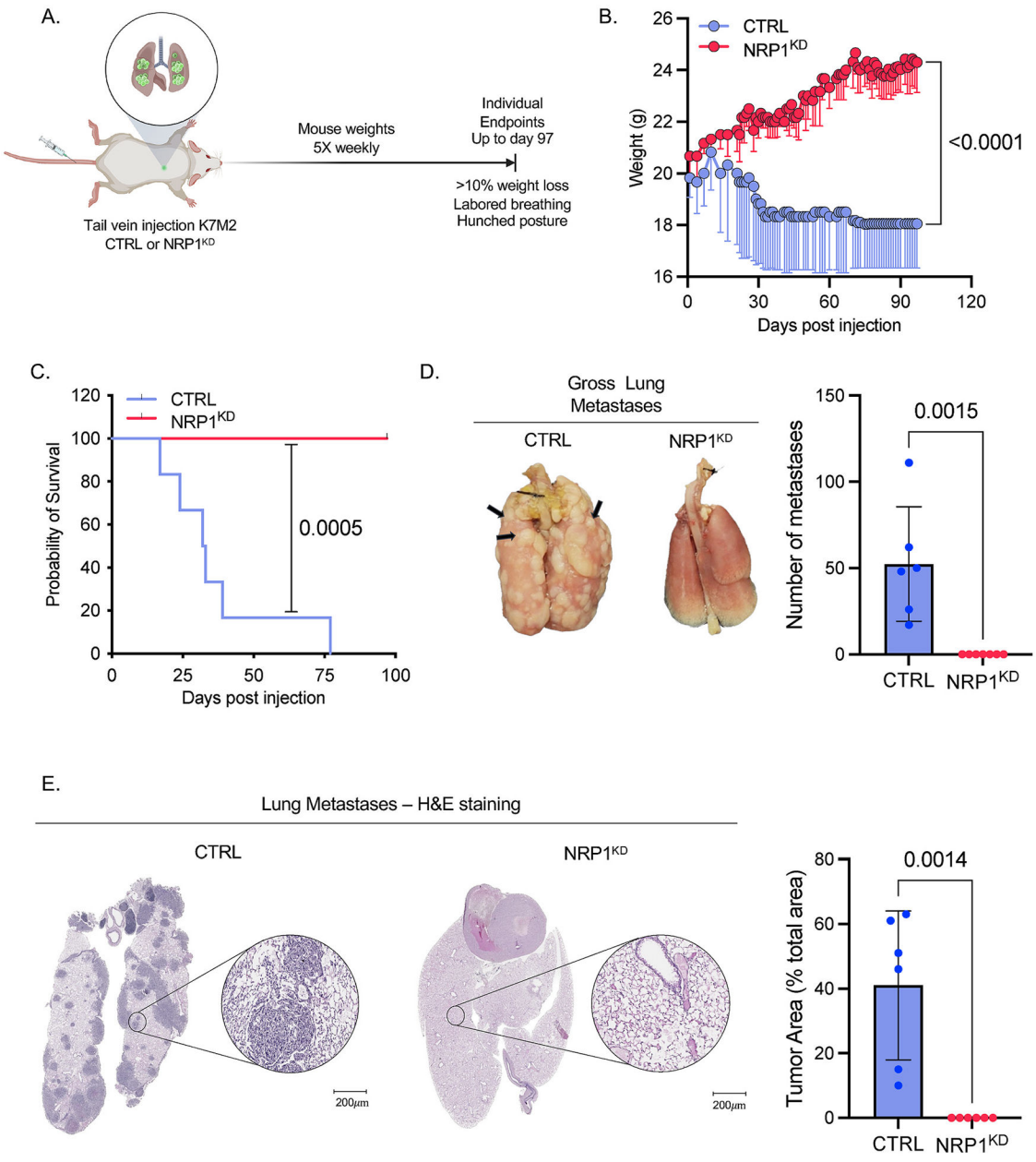

Fig. 4. Neuropilin-1 (NRP1) knockdown increases survival in mice.

A. Experimental design for survival study: K7M2 control shRNA and NRP1 shRNA cells were tail vein inoculated into immunocompetent BALB/c mice, mice were weighted five times per week and lungs were collected when mice reached individual endpoint. B. Weight of the mice (grams) injected with K7M2 control shRNA and NRP1 shRNA cells. C. Kaplan-Meier survival curve of time to reach clinical endpoint in the K7M2 control shRNA and NRP1 shRNA groups. D. When the mice reached the study endpoint, lungs from each group were inflated with Bouin's fixative solution and the number of surface metastases (mets; black arrows) were counted. Black arrows indicate surface metastases. E. Lung sections were stained with hematoxylin and eosin to analyze the percent tumor volume compared to

total volume of lungs section. Inset scale bar = 200 μm. CTRL denotes Control shRNA and $NRP1^{KD}$ denotes NRP1 shRNA.

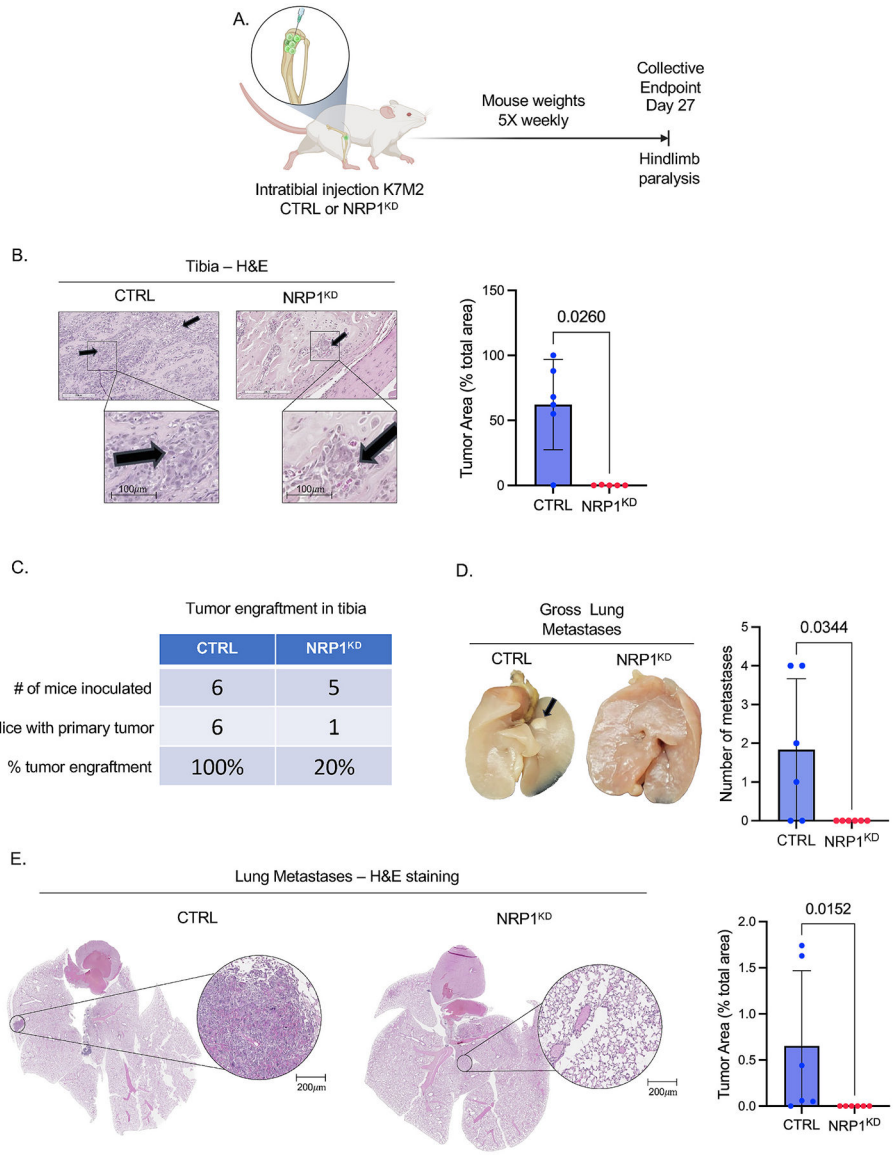

Fig. 5. Neuropilin-1 (NRP1) knockdown limits primary tumor engraftment.

A. Experimental design: K7M2 Control shRNA and K7M2 NRP1 shRNA cells were injected intratibially in BALB/c mice, mice were weighted five times per week, tibia and lungs were collected when mice reached collective endpoint on day 27. B. Hematoxylin and eosin staining of collected tibias to compare primary tumor burden between K7M2 Control shRNA and K7M2 NRP1 shRNA groups. Black arrows indicate OS. Inset Scale bar = 100 μm. C. Table showing percentage of primary tumor engraftment in both the groups based on H&E staining in tibia sections. D. Quantification of gross lung surface metastases = (mets; black arrows). Inset scale bar = 200 μm. E. Lung sections were stained with hematoxylin and eosin to analyze the percent tumor volume compared to total volume of lungs section. Inset scale bar = 200 μm. CTRL denotes Control shRNA and $NRP1^{KD}$ denotes NRP1 shRNA.

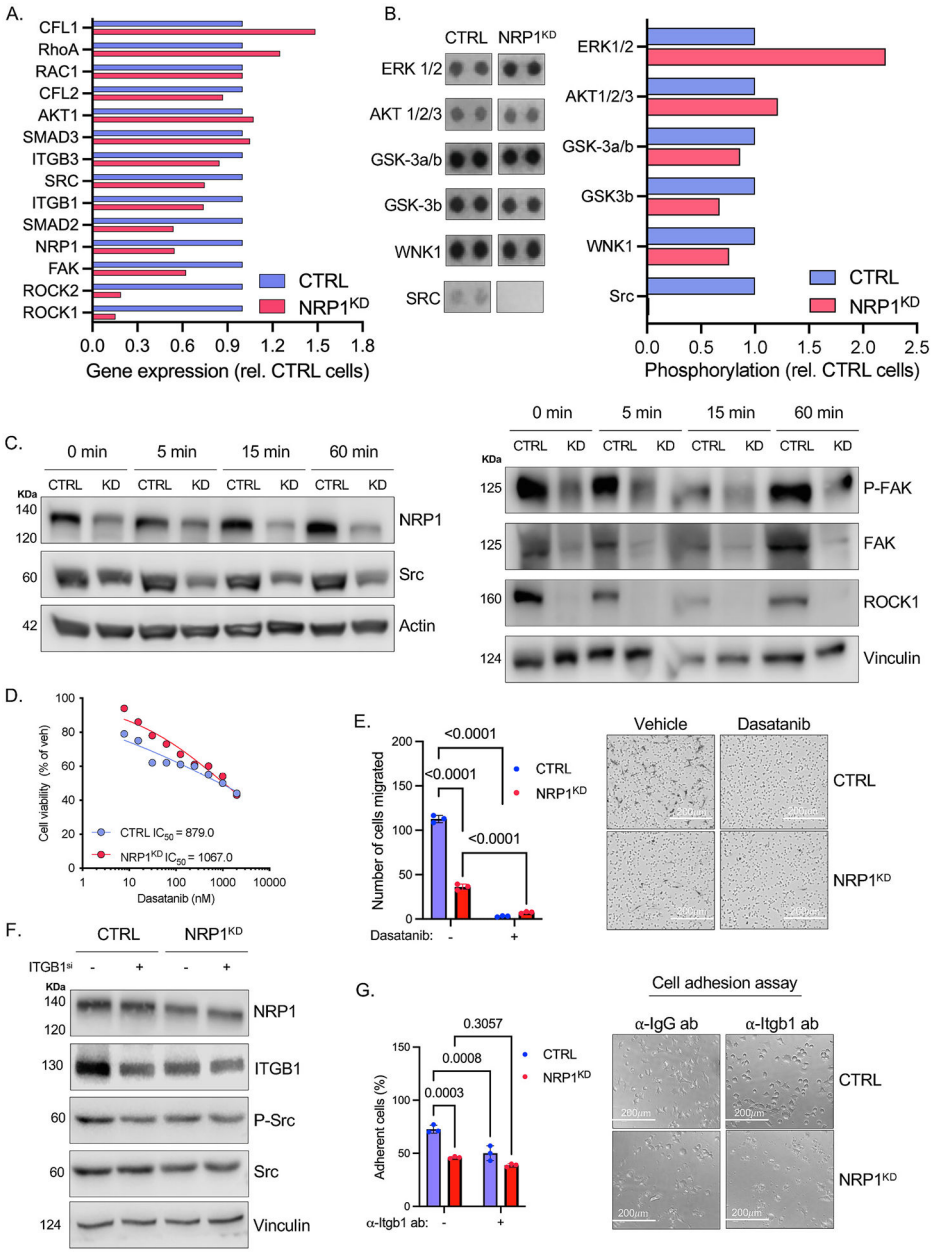

Fig. 6. NRP1 controls OS migration via SRC and ROCK.

A. Comparison of gene expression of NRP1 co-receptors or downstream effectors in K7M2 Control shRNA and NRP1 shRNA cells using qRT-PCR. B. Phospho-kinase array blots for different proteins and quantification comparing K7M2 Control shRNA and NRP1 shRNA cells. C. *In vitro* Western blot validation of downregulated proteins from A,B; Serum starved K7M2 Control shRNA and NRP1 shRNA cells samples were collected at different timepoints after treatment with 10 % serum containing media. D. Cytotoxicity assay showing IC_{50} values of dasatinib in K7M2 Control shRNA and NRP1 shRNA cells after 24 h. E. Quantification of Hematoxylin-stained images of migrated cells in K7M2 Control and NRP1 shRNA cells after dasatinib treatment. F. Western blot showing the effect of ITGB1 silencing in K7M2 Control and NRP1 shRNA cells on NRP1 and its downstream

effector proteins at 72h after siRNA transfection. G. Quantification of 20X microscopy images containing adhered cells in K7M2 Control and NRP1 shRNA cells after incubation with IgG/anti-integrin beta1 antibody (α-Itgb1 ab) in a fibronectin coated 96 well plate at 1-h timepoint. CTRL denotes Control shRNA, $NRP1^{KD}$ denotes NRP1 shRNA, KD denotes knockdown and $ITGB1^{si}$ denotes ITGB1 siRNA.